International Journal of Computational Fluid Dynamics, Vol. 21, No. 1, January 2007, 29–36

Taylor & Francis
Taylor & Francis Group

Finite element analysis of three-dimensional vortical flow structure and topology inside a carotid bifurcation model

S. F. TSAI†¶ and TONY W. H. SHEU‡*

†Department of Marine Engineering, National Taiwan Ocean University, No. 2, Pei-Ning Road, Keelung, Taiwan 202, Republic of China
‡Department of Engineering Science and Ocean Engineering, National Taiwan University, No. 1, Sec. 4, Roosevelt Road, Taipei, Taiwan 106, Republic of China

(Received 21 May 2006; in final form 11 March 2007)

Three-dimensional analysis of blood flow in the human carotid bifurcation model has been made using the streamline upwind Petrov-Galerkin finite element model. The primary aim of this study is to gain some insights into complex hemodynamics based on the topology theory. In addition, the preferential sites of atherosclerosis in the carotid model are predicted by virtue of the simulated critical lines.

Keywords: Carotid bifurcation; Three-dimensional; Streamline upwind Petrov-Galerkin; Topology theory; Critical lines

1. Introduction

In the human body, the carotid artery is important in supplying blood to the head and neck. The common carotid artery on the left side arises directly from the aortic arch; while on the right, it arises from the innominate artery. They ascend towards the thyroid cartilage and divide into the internal carotid and the external carotid. The internal carotid supplies blood to the cerebrum, forehead, nose, eye and middle ear. As for the external carotid, it sends branches to the face, scalp and neck.

Like many large arteries, the carotid artery bifurcates into branches. Clinical evidence strongly indicates that these bifurcations are the preferential sites where initial intimal thickening may occur. The low density lipoprotein tends to accumulate in the intima (Fry 1968, Ku *et al.* 1985). Eventually, the atherosclerotic lesion may result in local occlusions. Such hemodynamics in carotid bifurcation are believed to play a key role in atherosclerotic plague formation (Caro *et al.* 1971, Friedman *et al.* 1981, Zarins *et al.* 1983, Nerem 1992) for several reasons. On the one hand, atherosclerotic plague tends to form in regions with low shear stresses. The zones susceptible to such lesions are often found in the proximity of inner bend and on the nondivider wall of bifurcations. In large arteries, bifurcated regions are featured with the transient wall shear stresses and higher probability of developing atherosclerosis with initial intimal thickening. The resulting plague formation may constrict blood vessels and lead to myocardial infarction, stroke or limb loss. To gain knowledge of the arterial blood flow movement is, thus, useful for the detection of atherosclerosis in the early stage of disease by means of different noninvasive methods (Barnes *et al.* 1982, Roederer *et al.* 1984).

Blood flow patterns have long been known to be related to atherogenesis by Rindfleisch in 1872 (Rindfleisch 1872). To gain detailed insight into the complex hemodynamic pattern in carotid arteries, numerous experimental studies, predominantly *in vitro*, have been conducted (Bharadvaj *et al.* 1982a, Ku *et al.* 1985, Ku and Giddens 1987). The time-consuming nature of experimental measurements has made the use of numerical methods attractive. In the early days, investigations of hemodynamics in the carotid artery were mainly two-dimensional (Bharadvaj *et al.* 1982a,b, Perktold and Hilbert 1986, Kleinstreuer *et al.* 1991). More recently, three-dimensional hemodynamic analysis of the human carotid model has become increasingly feasible thanks to ever-improving hardware and software developments. Investigations have been carried out under steady flow conditions (Rindt 1989, Rindt *et al.* 1990) as well as under physiological pulsatile flow conditions (Perktold *et al.*

*Corresponding author. Tel.: + 886-2-33665746. Fax: + 886-2-23929885. Email: twhsheu@ntu.edu.tw
¶Tel.: +886-2-24622192. Ext. 7130. Fax: +886-2-24633765. Email: sftsai@ntou.edu.tw

International Journal of Computational Fluid Dynamics
ISSN 1061-8562 print/ISSN 1029-0257 online © 2007 Taylor & Francis
http://www.tandf.co.uk/journals
DOI: 10.1080/10618560701369569

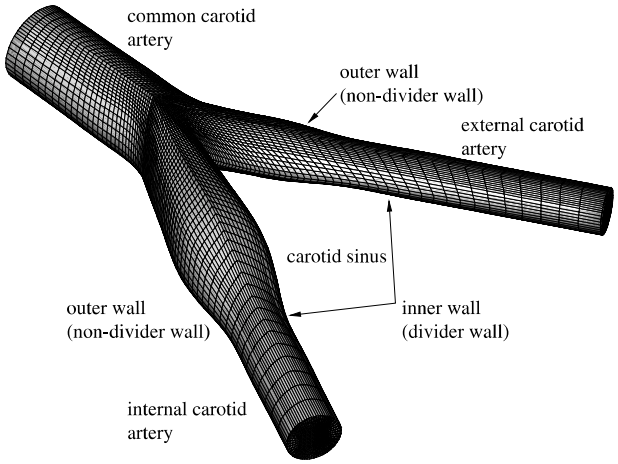

Figure 1. Schematic of the carotid model and surface meshes.

1991a, Rindt and Steenhoven 1996, Jou and Berger 1998, Gijsen *et al.* 1999). For more details about this subject, see reference (Perktold and Hofer 1999).

In the present work, the working equations in primitive variables and boundary conditions for pressure are described in section 2. This is followed by presenting the employed three-dimensional mixed finite element model. For the sake of stability, the test function is properly chosen so that stabilizing terms are added along the streamline direction. For the sake of accuracy, the amount of upwinding is determined in a way that the convection-diffusion equation can be obtained analytically within the one-dimensional context. In addition, the validity of employing the streamline upwind finite element model developed on triquadratic elements is shown. Section 3 presents the detailed vessel configurations and flow conditions. In section 4, investigation into the blood flow is emphasized on the formation of secondary flow and flow reversal. The rigorous theory is applied to theoretically determine the critical topology lines on the vessel wall. Finally, we provide some concluding remarks in section 5.

2. Numerical model

Computational analysis of blood flow in the anatomy schematic in figure 1 requires solving the three-dimensional viscous flow equations. Owing to ventricular systoles and diastoles (Ku *et al.* 1985), the blood flow in carotid artery is pulsatile in nature. As our goal is to understand the primary hemodynamics at the bifurcation site, the blood flow transport equations are assumed to be steady. With the exception in the proximal aorta and the aortic arch, the arterial flow is laminar once it leaves the aorta and proceeds toward the carotid, coronary and femoral arteries (Caro *et al.* 1978, Nichols and O'Rourke 1990). Besides the laminar flow assumption, both rigid wall assumption for the blood vessel and shear-thinning-free rheology assumption for blood fluid are made in order to simplify the analysis. The reason for neglecting arterial compliance is that the vessel elasticity is generally thought to have modest effect on the wall shear stress distribution (Zarins *et al.* 1983, Steinman and Ethier 1994, Perktold and Rappitsch 1995). Blood is, in fact, complex in composition and is of the non-Newtonian shear-thinning type (Thurston 1979). In light of previous studies (Bharadvaj *et al.* 1982b, Perktold *et al.* 1991b, Ballyk *et al.* 1994, Perktold *et al.* 1994), which clearly indicated that the non-Newtonian fluid behaviour is only of minor significance in large arteries, we assume that the flow in the carotid artery is of the Newtonian type. Under the incompressible and steady assumptions made for the

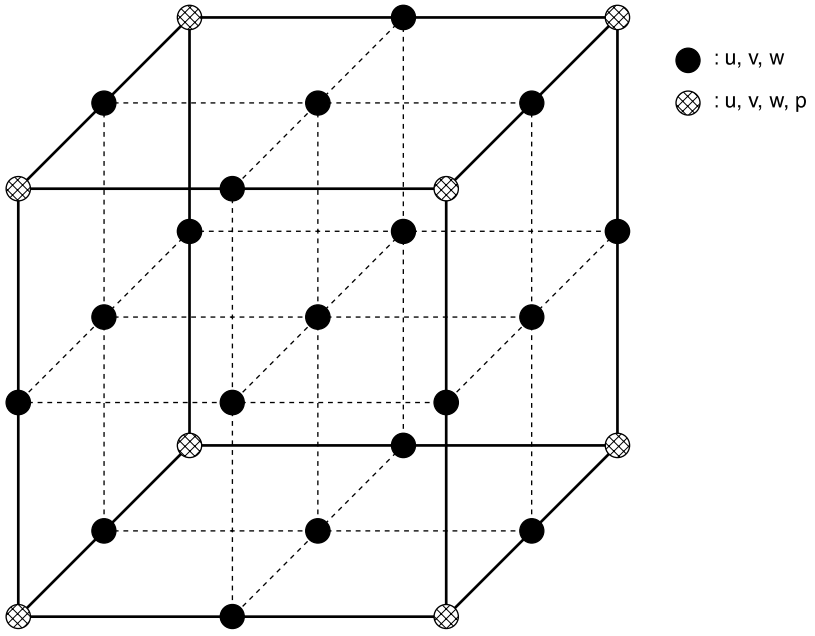

Figure 2. Schematic of the primitive variable storage in the tri-quadratic element.

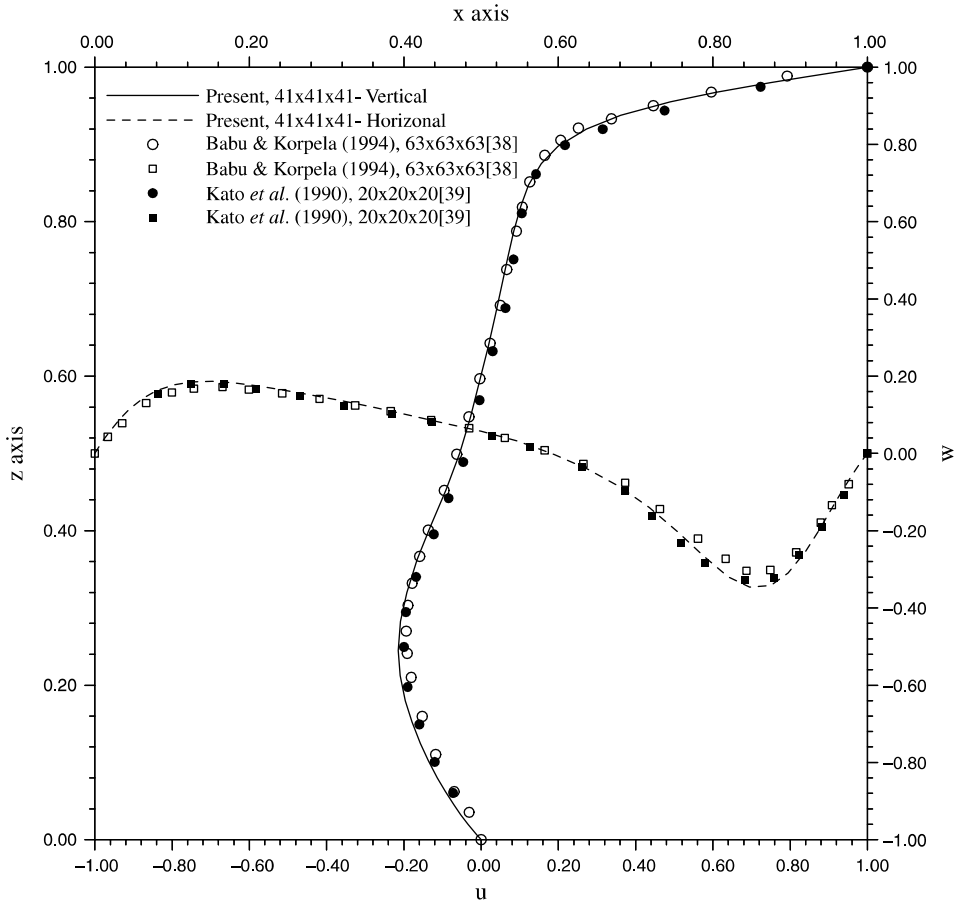

Figure 3. Comparison of the simulated mid-plane velocities with other predicted solutions.

current hemodynamic simulation, the continuity and Navier–Stokes equations in Cartesian coordinates are as follows:

$$\frac{\partial u_i}{\partial x_i} = 0 \tag{1}$$

$$\frac{\partial}{\partial x_m}(u_m u_i) = -\frac{\partial p}{\partial x_i} + \frac{1}{Re}\frac{\partial^2 u_i}{\partial x_m \partial x_m}. \tag{2}$$

The primitive-variable formulation is theoretically more advantageous due to its accommodated rigorous boundary conditions (Ladyzhenskaya 1963). For the sake of generality, the above differential system is normalized in a way that all the lengths are scaled by the hydraulic diameter of the blood vessel l_{ref}, and the velocity components u_{ref} by the mean inlet velocity. The Reynolds number is, thus, defined as $Re = ((u_{\text{ref}} l_{\text{ref}})/\nu)$, where ν is the kinematic viscosity of the blood fluid.

The weak solutions to equations (1)–(2) are obtained from the weighted residuals statement given below: Given admissive functions $\underline{w} \in H_0^1(\Omega) \times H_0^1(\Omega)$ and $q \in L_0^2(\Omega)$, we seek $\underline{u} \in H_0^1(\Omega)$ and $p \in L_0^2(\Omega)$ in a simply-connected

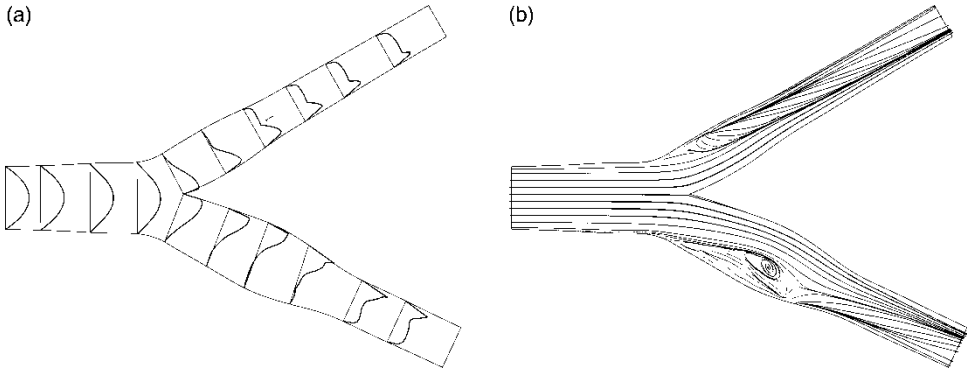

Figure 4. (a) The simulated streamwise velocity profiles on the bifurcation plane; (b) the simulated streamline on the bifurcation plane.

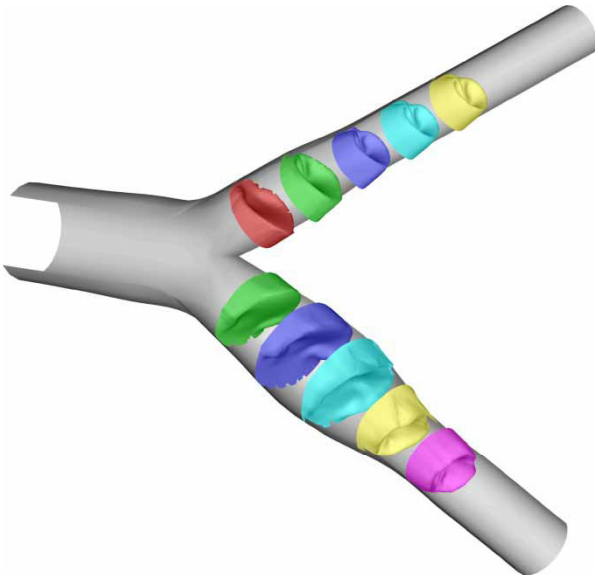

Figure 5. The simulated three-dimensional axial velocity in the carotid vessel.

domain Ω from

$$\int_\Omega (\underline{u}\cdot\nabla)\underline{u}\cdot\underline{w}\,\mathrm{d}\Omega + \frac{1}{Re}\int_\Omega \nabla\underline{u} : \nabla\underline{w}\,\mathrm{d}\Omega - \int_\Omega p\nabla\cdot\underline{w}\,\mathrm{d}\Omega = \int_{\Gamma/\Gamma_n} r\underline{w}\cdot\underline{n}\,\mathrm{d}\Gamma + \int_{\Gamma/\Gamma_\gamma} \underline{s}\cdot\underline{w}\times\underline{n}\,\mathrm{d}\Gamma \tag{3}$$

$$\int_\Omega (\nabla\cdot\underline{u})q\,\mathrm{d}\Omega = 0. \tag{4}$$

The boundary integral shown in equation (3) involves the surface integration on $\Gamma/\Gamma_{n,r}$, which denotes the complement of $\Gamma_{n,r}$ in $\Gamma = \partial\Omega$. For a field variable ϕ, $\underline{\phi} \in \Gamma/\Gamma_i (i = n, r)$ implies that $\underline{\phi} \in \Gamma$ but $\underline{\phi} \notin \Gamma_i$. In the above, $\underline{n}$ denotes the unit outward vector normal to Γ. In equation (3), $r = -p + (1/Re)\underline{n}\cdot\nabla\underline{u}\cdot\underline{n}$ and $\underline{s} = (1/Re)\underline{n}\cdot\nabla\underline{u}\times\underline{n}$.

The basis functions chosen to approximate the primitive variables are essential when conducting the mixed finite element analysis of incompressible equations. The *LBB* (or *inf-sup*) condition is the guiding principle for choosing the basis spaces for ($\underline{u}$, p) (Babuška 1971, Brezzi and Douglas 1988). The element schematically shown in figure 2 accommodates the *inf-sup* div-stability condition and will be employed in the present study. This element setting involves tri-quadratic polynomials $N^i (i = 1 \sim 27)$ for $\underline{u}$ and tri-linear polynomials $M^i (i = 1 \sim 9)$ for the p.

Prediction of flows at a Peclet number (or cell Reynolds number) larger than 2 requires careful approximation of advective terms in the momentum equations. Stability can be enhanced through a biased polynomial added on the top of the shape function (Hughes 1979). As a result, all nodal values at the upwind side need favourable consideration. Upwind schemes applied in the multi-dimensional analyses are, however, prone to numerical contamination due to the introduced false diffusion errors (Patankar 1980). To eliminate the resulting crosswind diffusion error without sacrificing convective stability, our previously developed quadratic finite element model will be applied so that the stabilizing term is added along the flow direction for the enhancement of the discrete system (Sheu *et al.* 2000).

Within the mixed finite element framework, the storage requirement may exceed the capacity of today's computers. For this reason, the Lanczos-based BiCGSTAB iterative solver (Von der Vorst 1992) is employed to tackle unsymmetric matrix equations. Beside the ability of avoiding irregular convergence, BiCGSTAB can locally minimize the residuals by virtue of GMRES (1). Another advantage of using the BiCGSTAB solver is to avoid dealing with the transpose of matrix equations. For computational efficiency, the element-by-element capability has been built into the chosen iterative solver. The reader can refer to the work of Wang and Sheu (1997) for additional details about the implementation of EBE-BiCGSTAB solution algorithm. As is usual, the integrity of the employing the three-dimensional Petrov-Galerkin finite element code for incompressible flow

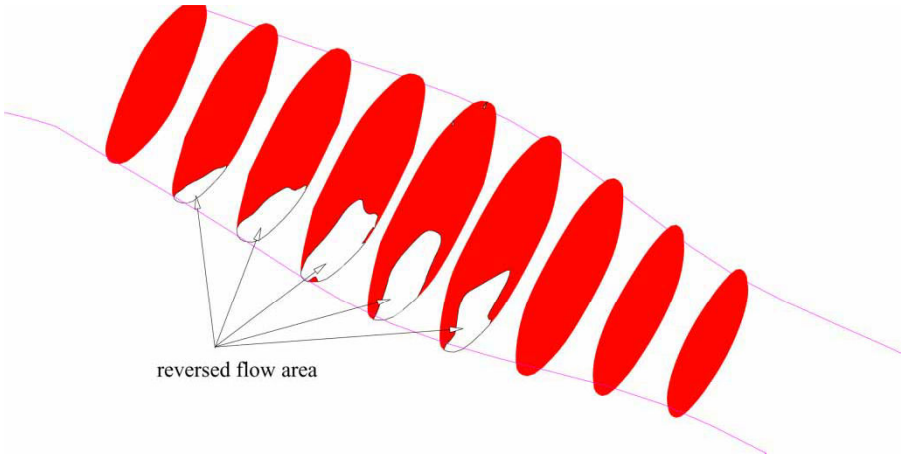

Figure 6. The simulated three-dimensional reversed flow regions in the carotid sinus.

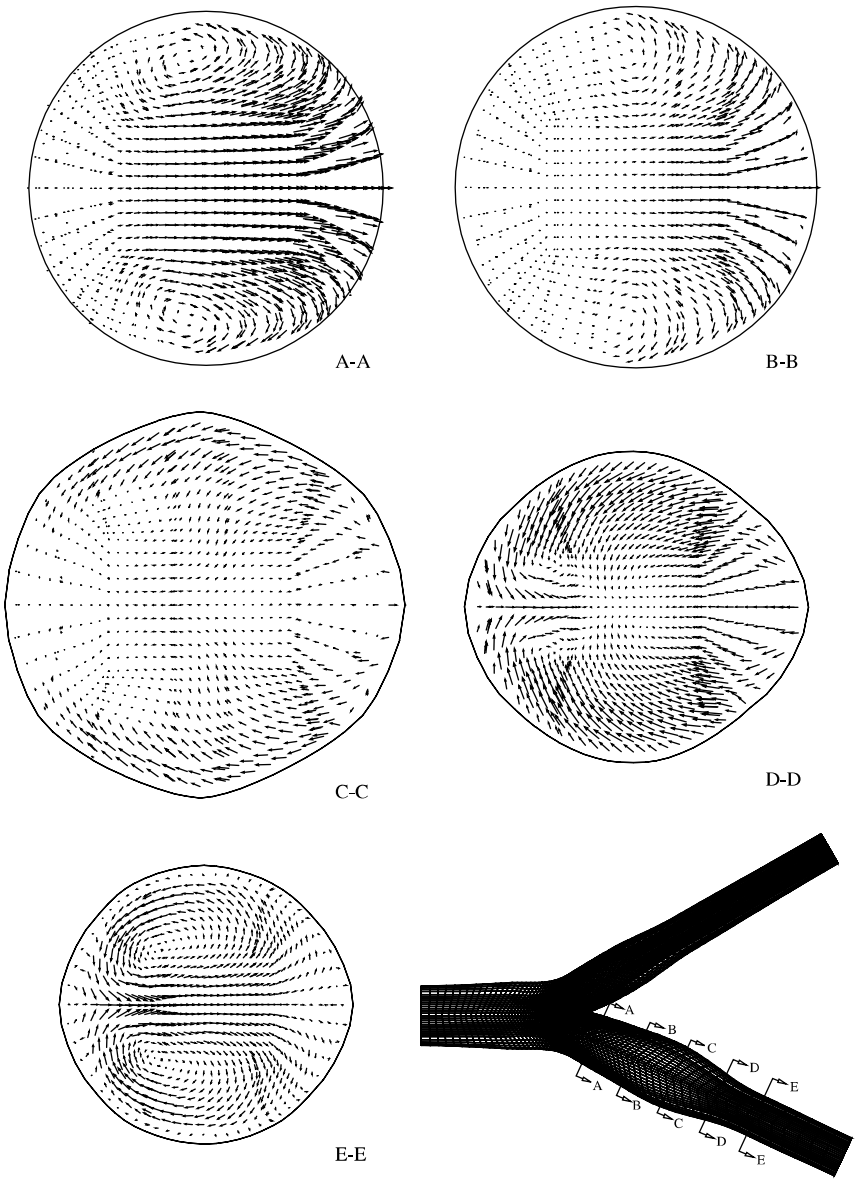

Figure 7. The simulated secondary flow patterns at five chosen cross planes.

equations is validated by solving lid-driven cavity problem in a cubic of unit length at $Re = 400$. The simulated results show good agreement with the simulated velocity profiles of Babu and Korpela (1994) and Kato *et al.* (1990) in figure 3.

3. Problem description

To facilitate the discussion of results, the plane of symmetry is denoted as the branching plane of the investigated carotid rigid model. As atherosclerotic plaque occurs preferentially in the regions of nondivider walls of bifurcation (Zarins *et al.* 1983, Ku *et al.* 1985), it is instructive to define the inner (divider) and the outer (non-divider) wall as schematically shown in figure 1. Under the Newtonian flow assumption, the entry blood flow of $\nu = 2.83 \times 10^{-6}\,\mathrm{m^2\,s^{-1}}$ ($\nu = \mu/\rho$, where $\rho = 1060\,\mathrm{kg\,m^{-3}}$ and $\mu = 3 \times 10^{-3}\,\mathrm{Pa\,s}$) is assumed to be of the non-pulsatile type with the flow rate of $\dot{Q} = 0.8\,\mathrm{l/min}$. The resulting Reynolds number for this blood fluid, which is 500, falls into the laminar flow regime.

It is well known that the simulation quality depends greatly on the grid distribution. It is, therefore, desirable to avoid excessive grid distortion in the current simulation. To provide a smoothly distributed mesh for the bifurcation vessel under current investigation, we discretize the physical domain within the multi-block context. On physical grounds, grids should be refined in regions immediately adjacent to the vessel walls as well as in the bifurcated zone. Bearing this in mind, the grids shown in figure 1 were properly constructed in 24 blocks to yield a total number of 112,585 well-meshed points.

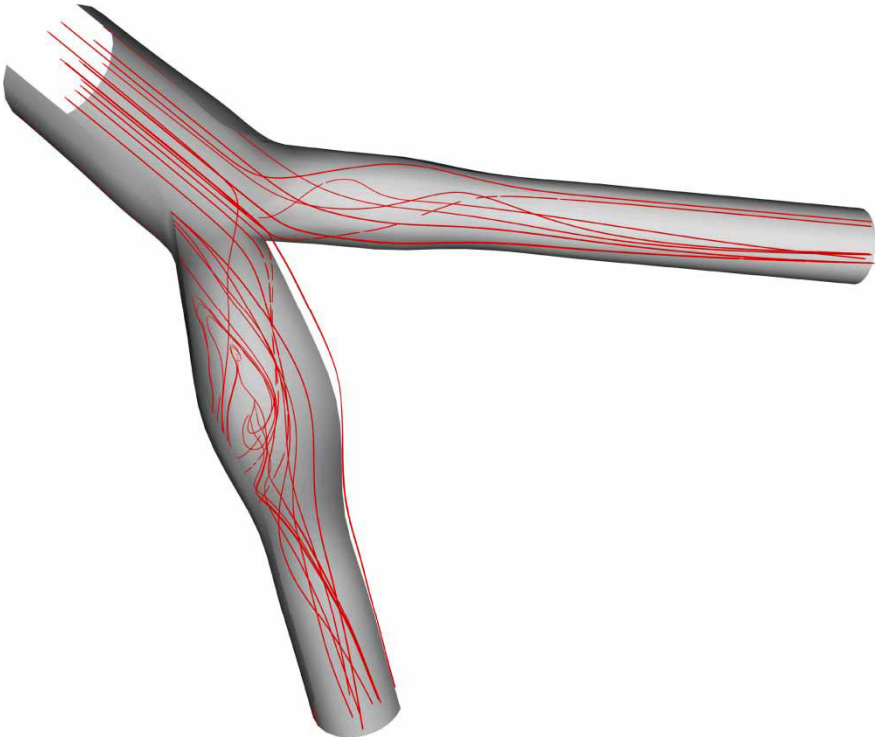

Figure 8. The simulated particle tracers in the carotid vessel.

To close the differential system of the working equations, boundary conditions should be prescribed on the entry plane, exit planes and vessel walls. At a given flow rate, we assumed that the blood flow at the entry plane has been fully-developed. The traction free outflow condition given below can then be applied (Perktold and Hofer 1999):

$$-p\delta_{ij} + \frac{1}{Re}(u_{i,j} + u_{j,i})n_j = 0 \quad (i,j = 1,2,3). \qquad (5)$$

In the above, n_j denotes the j component of the unit outward vector at the outlet planes. In addition, the

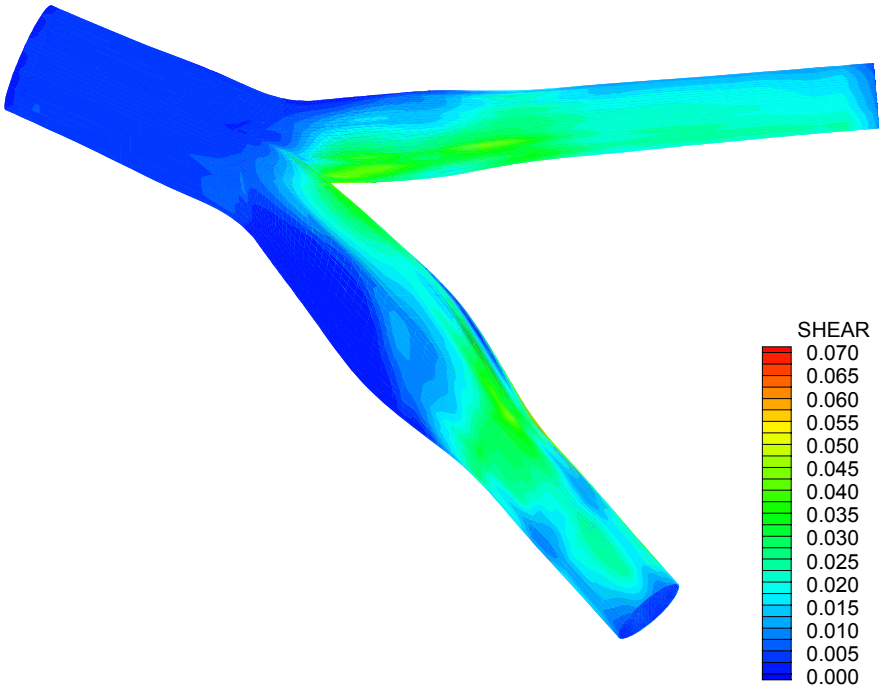

Figure 9. The simulated three-dimensional contours of the wall shear stresses.

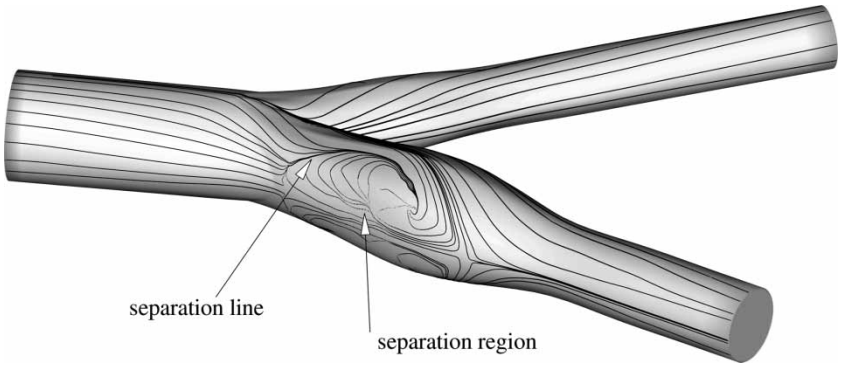

Figure 10. The simulated three-dimensional lines of separation.

tangential force vector of zero magnitude is applied at the two truncated exit planes.

4. Computed results

To provide evidence that the clinically observed flow reversal indeed occurs preferentially in the regions of bifurcation, the simulated velocities and streamlines are plotted on the branching plane of the carotid vessel. Figure 4(a) shows that the velocity profiles are skewed in the two branches in the direction of the divider wall. Such shewness in the vessel configuration results in a higher velocity gradient near the inner wall but yields a rather small velocity gradient near the outer wall. It is, thus, possible to observe backward motion with a substantial stagnation in the outer sinus region. The zone of flow reversal, as shown in Figure 4(b), is indeed located in the widened segment of the internal carotid (or the carotid sinus). This confirms that the carotid sinus is a zone of crucial hemodynamic importance owing to the resulting greater probability of atheroclerotic lesion in the artery. At the entrance to the internal and external carotids, the simulated flow moving towards the divider wall is due to the branching and curvature effects.

To illustrate the three-dimensional zone with reversed axial flow near the outer wall of the carotid sinus, we plot in figure 5 the velocity profiles at some selected streamwise cross sections of the common carotid, internal and carotid arteries. In the common carotid artery, upstream of the branching point the entry flow retains symmetry rather well. The axial velocity of larger magnitude and higher velocity gradient can be clearly seen near the divider wall. In the widened sinus of the investigated internal carotid, the regions of stagnating and reversed extend from the outer artery wall. Downstream of the bifurcation point, the peak velocity shifts towards the inner walls of the internal/external carotid arteries, whereas the axial velocity of smaller magnitude appears at the outer walls, especially near the outer wall in the internal carotid artery. To depict the possibility of three-dimensional flow reversal, zones of reversed flow at the flow cross-sections are plotted in the figure 6. In the external carotid, no lines of zero axial velocity are seen and, thus, no reversed flow will show its presence. On the contrary, flow reversal is clearly seen in the sinus. Outside of the sinus, no flow separation is ever observed.

Figure 7 shows that the secondary motion in the core proceeds towards the outer side of the curvature, whereas the fluid particle near the wall is directed towards the inner curvature wall. This distinguished flow feature is known to result from the centrifugal force in a curved vessel. Secondary flow motion can be more clearly illustrated by the simulated trajectory of the seeded massless fluid particles at the entry plane. These fluid markers are seen to spiral downwards. In figure 8, the spiralling nature of the flow motion in the sinus is attributed to the axial velocity component and the aforementioned secondary flow for motion.

Low shear stress is now well accepted as one of the major hemodynamic risk factor for various vascular diseases since the region with low shear stress is susceptible to blood circulation. The accompanying high particle residence time turns out to be a natural mechanism for stenosis. The importance of the resulting wall shear stresses motivates us to plot their contours in figure 9. On the investigated carotid artery wall, the wall shear stresses on the outer wall of the internal carotid sinus are relatively smaller in magnitude. This confirms that the outer wall of the internal carotid sinus is susceptible to atherosclerotic lesions.

In light of the effect of separated flow on the carotid artery, it is rational to identify the locations where the blood will be separated flow and is then attached to the vessel wall. In this study we apply the topology theory to determine the lines of separation and reattachment on the three-dimensional vessel walls (Legendre 1956, Sheu *et al.* 2000, Chiang *et al.* 2000). Based on the simulated critical lines plotted in figure 10, the zone in the vicinity of the carotid sinus is seen to be marked by the simulated lines of separation and reattachment. The presence of these critical lines explains flow entrainment into the recirculating region and its subsequent obstruction in the internal carotid artery.

5. Conclusions

In this paper, the Navier–Stokes equations for the non-pulsatile incompressible Newtonian blood flow has been

solved within the streamline upwind framework for the sake of stability. The employed convectively very stable finite element model has been shown to be accurate in the sense that an analytic solution can be obtained in the limiting one-dimensional case. The simulated three-dimensional results reveal the regions with low shear stresses and show that they are located on the nondivider walls of bifurcation. In view of the particle tracers which show the complex spiralling flow field in the carotid artery, we conclude that the carotid sinus in the internal carotid artery is susceptible to atherosclerotic lesions. The flow complexity results from the shift of the axial velocity towards the inner walls and the rapidly developing secondary flow in the internal and external carotid arteries downstream of the bifurcation point. To accurately indicate where the flow is separated and reattached, the rigorous topology theory is employed to determine the critical lines based on the simulated limiting streamlines.

Acknowledgements

Financial support provided by the National Science Council under Grant NSC94-2611-E-002-021- is gratefully acknowledged.

References

Babu, V. and Korpela, S.A., Numerical solution of the incompressible three-dimensional Navier–Stokes equations. *Comput. Fluids*, 1994, **23**(5), 675–691.

Babuška, I., Error bounds for finite element methods. *Numer. Math.*, 1971, **16**, 322–333.

Ballyk, P.D., Steinman, D.A. and Ethier, C.R., Simulation of non-Newtonian blood flow in an end-to-side anastomosis. *Biorheology*, 1994, **31**, 565–586.

Barnes, R.W., Rittgers, S.E. and Puttney, W.W., Real-time Doppler spectrum analysis predictive value in defining operable carotid artery disease. *Arch. Surg.*, 1982, **117**, 52–57.

Bharadvaj, B.K., Mabon, R.F. and Giddens, D.P., Steady flow in a model of human carotid bifurcation. Part II: Laser-Doppler measurement. *J. Biomech.*, 1982a, **15**(5), 363–378.

Bharadvaj, B.K., Mabon, R.F. and Giddens, D.P., Steady flow in a model of human carotid bifurcation. Part I: flow visualization. *J. Biomech.*, 1982b, **15**(5), 349–362.

Brezzi, F. and Douglas, J., Stabilized mixed methods for the Stokes problem. *Numer. Math.*, 1988, **53**, 225–235.

Caro, C.G., Fitzgerald, J.M. and Schroter, R.C., Atheroma and arterial wall shear observations correlation and proposal of a shear dependent mass transfer mechanism for atherogenesis. *Proc. R. Soc. Lond. Ser. B. Biol. Sci.*, 1971, **17**(7), 109–159.

Caro, C.F., Pedley, T.J., Schorter, R.C. and Seed, W.A., *The Mechanics of the Circulation*, 1978 (Oxford University Press: Oxford).

Chiang, T.P., Sheu, T.W.H. and Wang, S.K., Side wall effects on the structure of laminar flow over a plane-symmetric sudden expansion. *Comput. Fluids*, 2000, **29**(5), 467–492.

Friedman, M.F., Peters, O.J., Bargero, C.B., Hutchins, G.M. and Mark, F.F., Correlation between intimal thickness and fluid shear in human arteries. *Atherosclerosis*, 1981, **39**, 425–436.

Fry, D.L., Mass transport, atherogenesis and risk. *Arteriosclerosis*, 1968, **7**, 88–100.

Gijsen, F.J.H., van de Vosse, F.N. and Janssen, J.D., The influence of the non-Newtonian properties of blood on the flow in larger arteries: steady flow in a carotid bifurcation model. *J. Biomech.*, 1999, **32**, 601–608.

Hughes, T.J.R., *Finite Element Methods for Convection Dominated Flows, AMD*, Vol. 34, 1979 (ASME: New York).

Jou, L.D. and Berger, S.A., Numerical simulation of the flow in the carotid bifurcation. *Theoret. Comput. Fluid Dynamics*, 1998, **10**, 239–248.

Kato, Y., Kawai, H. and Tanahashi, T., Numerical flow analysis in a cubic cavity by the GSMAC finite-element method. *JSME Int. J. Ser. II*, 1990, **33**, 649–658.

Kleinstreuer, C., Nazemi, M. and Archie, J.P., Hemodynamics analysis of a stenosed carotid bifurcation and its plaque-mitigating design. *J. Biomech. Eng.*, 1991, **113**, 330–335.

Ku, D.K. and Giddens, D.P., Laser Doppler anemometer measurements of pulsatile flow in a model carotid bifurcation. *J. Biomech.*, 1987, **20**, 407–421.

Ku, D.N., Giddens, D.P., Zarins, C.K. and Glagov, S., Pulsatile flow and atherosclerosis in the human carotid bifurcation, positive correlation between plaque location and low oscillating shear stress. *Arteriosclerosis*, 1985, **5**(3), 293–302.

Ladyzhenskaya, O.A., *Mathematical Problems in the Dynamics of a Viscous Incompressible Flow*, 1963 (Gordon and Breach: New York).

Legendre, R., Séparation de courant Íéconlment laminaire tridimensional. *Rech. Aéro*, 1956, **54**, 3–8.

Nerem, R.M., Vascular fluid mechanics, the arterial wall, and atherosclerosis. *J. Biomech. Eng.*, 1992, **114**, 274–282.

Nichols, W.W. and O'Rourke, M.F., *McDonald's Blood Flow in Arteries*, 3rd ed., 1990 (Lea & Febiger: Philadephia).

Patankar, S.V., *Numerical Heat Transfer and Fluid Flow*, 1980 (Hemisphere: Washington, D C).

Perktold, K. and Hilbert, D., Numerical simulation of pulsatile flow in a carotid bifurcation model. *J. Biomech. Eng.*, 1986, **8**, 193–199.

Perktold, K. and Hofer, M., Mathematical modelling of flow effects and transport processes in arterial bifurcation models. In *Haemodynamics of Arterial Organs*, edited by X.Y. Xu and M.W. Collins, pp. 42–84, 1999 (WIT Press: Southampton).

Perktold, K. and Rappitsch, G., Computer simulation of local blood flow and vessel mechanics in a compliant carotid artery bifurcation model. *J. Biomech.*, 1995, **28**(7), 845–856.

Perktold, K., Resch, M. and Peter, R.O., Three-dimensional numerical analysis of pulsatile flow and wall shear stress in the carotid artery bifurcation. *J. Biomech.*, 1991a, **24**(6), 409–420.

Perktold, K., Resch, M. and Florian, H., Pulsatile non-Newtonian flow characteristics in a three-dimensional human carotid bifurcation model. *J. Biomech. Eng.*, 1991b, **113**, 464–475.

Perktold, K., Thurner, E. and Kemer, T., Flow and stress characteristics in rigid walled and compliant carotid artery bifurcation models. *Med. Biol. Eng. Comput.*, 1994, **32**, 19–26.

Rindfleisch, E., *Manual of Patheological Histology*, Vol. 1, 1872 (New Sydenham Society: London).

Rindt, C.C.M., *Analysis of the Three-Dimensional Flow Field in the Carotid Bifurcation*, PhD Thesis. University of Technology: Eindhoven, 1989.

Rindt, C.C.M. and Steenhoven, A.A.V., Unsteady flow in a rigid 3-D model of the carotid artery bifurcation. *J. Biomech. Eng.*, 1996, **118**, 90–96.

Rindt, C.C.M., Steenhoven, A.A.V., Janssen, J.D., Reneman, R.S. and Segal, A., A numerical analysis of steady flow in a three-dimensional model of the carotid bifurcation. *J. Biomech.*, 1990, **23**, 461–473.

Roederer, G.O., Langlois, Y.E., Jager, K.A., Primozich, J.F., Beach, K.W., Phillips, D.J. and Strandness, D.E., The natural history of carotid arterial disease in asymptomatic patients with cervical bruits. *Stroke*, 1984, **15**, 605–613.

Sheu, T.W.H., Wang, M.M.T. and Tsai, S.F., Element by element parallel computation of incompressible Navier–Stokes equations in three dimensions. *SIAM J. Sci. Comput.*, 2000, **21**(4), 1387–1400.

Steinman, D.A. and Ethier, C.R., Numerical modelling of flow in a distensible end-to-side anastomosis. *J. Biomech. Eng.*, 1994, **116**, 295–301.

Thurston, G.B., Rheological parameters for the viscosity, visco-elasticity and thitropy of blood. *Biorheology*, 1979, **16**, 149–162.

Von der Vorst, H.A., BI-CGSTAB: A fast and smoothly converging variant of BI-CG for the solution of nonsymmetric linear systems. *SIAM J. Sci. Stat. Comput.*, 1992, **13**(2), 631–644.

Wang, M.M.T. and Sheu, T.W.H., An element-by-element BiCGSTAB iterative method for three-dimensional steady Navier–Stokes equations. *J. Comput. Appl. Math.*, 1997, **79**, 147–165.

Zarins, C.K., Giddens, D.P., Bharadvaj, B.K., Sottiural, V.S., Mabon, R.F. and Glagov, S., Carotid bifurcation atherosclerosis: quantitative correlation of plaque localization with flow velocity profiles and wall shear stress. *Circ. Res.*, 1983, **53**, 502–514.